Source Process of Deep and Intermediate Earthquakes as Inferred from Long-Period P and S Waveforms
1. Intermediate-depth Earthquakes in the Southwest Pacific Region

By
Takeshi MIKUMO
Disaster Prevention Research Institute, Kyoto University

Abstract

The source process of four intermediate earthquakes with magnitudes of 6.0-6.8 and focal depths between 100 and 200 km has been re-investigated from the analysis of long-period P and S waveforms.

The source process times recovered from the times of the first half cycle of recorded P waves or the group delay times derived from the slopes of equalized phase spectrum show an azimuthal dependence with respect to the orientation of a nodal plane and of the null vector. If we assume shear dislocation models for these earthquakes, the dependence yields a solution to the problem of which of two nodal planes corresponds to the slip plane. Various source parameters have also been estimated from the azimuthal dependence by least squares technique.

The dimension of the slip plane or the fault length and width range in 25-40 km and 8-18 km, respectively, and the rise time of dislocation is found to be about 1 sec. The rupture velocity might be as low as 3.2 km/sec, if two-dimensional propagation is assumed.

The theoretical seismograms of both direct P and S waves appropriate to each recording station have been synthesized on the basis of the estimated source parameters, taking into account the combined effects of wave propagation in the mantle and the crust and of the seismograph response. A good agreement of general features between the observed and synthesized waveforms on the three component seismograms gives support to the above slip dislocation model. Comparison of the amplitudes on the both kinds of seismograms yields seismic moment of the order of $1.6\text{-}3.0\times10^{26}$ dyne·cm and the amount of dislocation of 80-140 cm. The stress drop at these earthquakes ranges from 50 to 90 bars but might exceed 170 bars for one shock. The effective initial stress to produce shear dislocations is also estimated in relation to the frictional stress on the slip plane.

§ 1. Introduction

Recent seismic observations covering a low frequency range and the introduction of elastic dislocation models have provided a powerful approach to clarify the dynamical process at the source not only of large shallow earthquakes, but also of deep-focus and intermediate-depth earthquakes that occurred between 100 and 600 km (TENG and BEN-MENAHEM, 1965; BOLLINGER, 1968; BERCKHEMER and JACOB, 1968; MIKUMO, 1969; FUKAO, 1970). It is expected that if the source of all these earthquakes can be interpreted in terms of shear dislocations, the stress-strain drop at the source, shear stresses causing these earth quakes, and their variations with depth will be estimated, and that the strength and thermal state of material in the mantle and their implications to the tectonic structure of a deep seismic zone, such as descending slabs of the lithosphere (ISACKS *et al.*, 1968; MCKENZIE, 1969), and the cause of deep and intermediate earthquakes might be brought into the light.

It appears that there still remain unsolved problems on the observational side in an application of shear dislocation models to deep earthquakes. The problems are; whether the source is a moving dislocation, or at what velocity dislocations spread out over a slip plane formed in the mantle with increased temperature and pressure; and whether the radiation pattern of S waves including the absolute amplitudes and waveforms can be

explained by a dislocation source with the same parameters as for P waves.

The purpose of the present paper is to elucidate more clearly the source process of intermediate-depth earthquakes, by making direct approach to the problems. The first step is to make an attempt to estimate the source parameters including the dimension, the amount of dislocation and the rupture velocity, from azimuthal variations of recorded P waveforms. The second approach is to synthesize theoretical seismograms of both P and S waves from dislocation sources with the estimated parameters, taking into account the combined effects of wave propagation in the earth and a recording instrument, and to compare them with their observed waveforms on the three-component records, in order to test the appropriateness of the assumed model. The stress drop at the time of these earthquakes and the initial stress to produce shear dislocations are discussed in some detail.

§ 2. Data

The earthquakes analyzed here are four intermediate shocks that occurred along island arcs from New Guinea to the Fuji Islands at depths between 100 and 200 km, which have been treated in a previous paper (MIKUMO, 1969). Relevant information is again listed in Table 1. Data used are the long-period vertical and two horizontal component seismograms recorded at the WWSSN stations.

§ 3. Analysis

In the previous study (MIKUMO, 1969), theoretical seismograms of direct P waves have been synthesized from moving dislocation models with variously assumed source parameters through a linear filter system composed of the earth and instrument, and compared with the corresponding records. The comparison has shown that the average waveform on the records is similar to that from a double-couple point source with a ramp function time dependence with $\tau < 3$ sec, and yielded the seismic moment and probable ranges for some other parameters. Closer examinations reveal, however, some difference in the recorded P waveforms for the first half-period as well as in the slope of the equalized phase spectrum (MIKUMO 1969), depending on the location of recording stations with respect to the source. For this reason, an attempt is made here to evaluate the possible azimuthal dependence of the above two quantities. Although the waveforms are predominantly controlled by the seismograph characteristics, we assume that there are no serious differences in its frequency response among the stations. This assumption may be justified by the fact that the shape of calibration pulses placed on seismograms is almost identical at these stations.

(1) The slope of the phase spectrum (or the group delay time)

The equalized source phase spectrum of direct P waves has been given in Fig. 19 in the previous paper, for all stations in the four earthquakes mentioned. It can be seen that there are appreciable differences in the slope of the spectrum, and a possibility has been suggested that the source dimension could in principle be evaluated from the slopes if the initial phase correction is made for a spherical earth. The correction gives a constant term independent on frequency on the standpoint of normal modes (BRUNE, 1964; SATO, 1969), and hence yields no effects on the

Table 1. Information of the earthquakes analyzed.

Shock No.	Date	Origin time h m s	Location φ λ	Depth km	Magnitude	Plane A s. d.	Plane B s. d.
6	1963 July 4	10 58 13.2	26.3°S 177.7°W	158	6.5	107° 65°	211° 62°
12	1964 Jan. 20	17 18 37.4	20.7 S 169.9 E	141	6.8	75 61	139 52
15	1964 Apr. 24	05 56 10.1	5.1 S 144.2 E	106	6.8	171 83	171 6
23	1966 Feb. 4	10 39 12.2	15.9 S 167.9 E	190	6.3	37 86	127 82

slope of the phase spectrum. The corrected source phase $\tilde{\varphi}(\omega)$ in the case of unilateral faulting may be written (MIKUMO, 1969),

$$\tilde{\varphi}(\omega)=\varphi_{\dot{U}}(\omega)+\varphi_S(\omega)=\omega\tau/2+\omega(T_L+T_W)$$

and

$$T_L=\frac{L}{2}\left|\frac{1}{v}-\frac{\alpha_j}{v_p}\right|,\quad T_W=\frac{W}{2}\left|\frac{\alpha_k}{v_p}\right| \qquad (1)$$

where τ is the time constant of dislocation, L and W are the length and width of the slip plane, v_p and v are the compressional wave velocity and rupture velocity, and α_j and α_k are the direction cosines of the relevant ray relative either to the slip direction or to the null vector, respectively. The slope of the phase spectrum $d\tilde{\varphi}/d\omega$ or the group delay time is then related to the azimuth of the station and to the source parameters in the following form,

$$\frac{d\tilde{\varphi}}{d\omega}=\frac{1}{2}\left(\tau+L\left|\frac{1}{v}-\frac{\alpha_j}{v_p}\right|+W\left|\frac{\alpha_k}{v_p}\right|\right) \qquad (2)$$

The left-hand side can be determined from observations. Eq. (2) indicates that L/v_p, W/v_p and $\tau\pm L/v$ may be evaluated directly from the group delay times at more than three stations.

In the upper part of Figs. 1(a) (earthquake No. 23) and 1(b) (earthquake No. 15) are plotted the group delay times determined from the equalized phase spectra over the frequency range between 0.01 and 0.15 c/s. There appears to be some linear dependence of the plots with the azimuth to a possible slip direction in the earthquakes, but with rather large scattering. The reason for this might be be accounted for; i) The assumed crustal structures are not always appropriate for each station (the slopes have been cor-

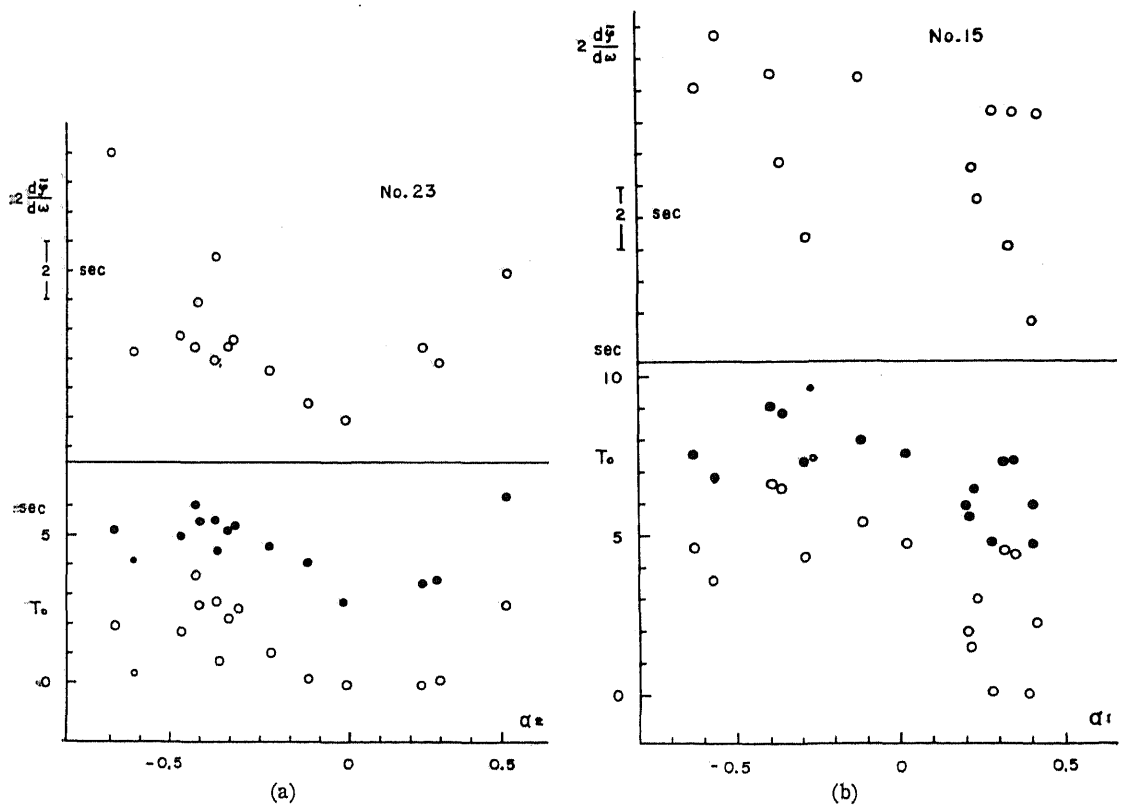

Fig. 1. Group delay times, observed first half-periods, and source process times.
(a) No. 15 (b) No. 23

rected for a standard structure of HASKELL (1960).). A difference of 10 km in the crustal thickness yields the change of about 1.5 sec in the group delay time. ii) The corrected phase spectra do not change monotonously with frequency; and iii) The initial time of digitization might not exactly agree with the arrival time of first P waves when they have a blunt beginning. It would therefore be rather difficult to rely on the group delay times in a precision determination of the source parameters.

(b) Source process time

Another method is to infer from observed records the apparent time duration of energy release at the source region or the total time of faulting process, which is specified by the source finiteness and the rise time of dislocation. The displacement of P waves $u_r^0(t)$ at great distances from dislocation sources may be expressed by (MIKUMO, 1969),

$$u_r^0(t)=\frac{1}{2\pi}\int_{-\infty}^{\infty}\dot{U}(\omega)\cdot S(\omega)e^{i\omega t}d\omega \qquad (3)$$

$$=\int_0^{\infty}\Delta\dot{u}(t')s(t-t')dt' \qquad (4)$$

where

$$\left.\begin{aligned}\dot{U}(\omega)&=\frac{D\sin(\omega\tau/2)}{\omega\tau/2}\exp(-i\omega\tau/2),\\ \Delta\dot{u}(t)&=\frac{D}{\tau}\Big[H(t)-H(t-\tau)\Big]\end{aligned}\right\} \qquad (5)$$

$$\left.\begin{aligned}S(\omega)&=S_0\cdot S_L(\omega)\cdot S_W(\omega),\\ s(t)&=S_0\int_0^{\infty}s_L(t')s_W(t-t')dt'\end{aligned}\right\} \qquad (6)$$

$$\left.\begin{aligned}S_{L,W}(\omega)&=\frac{\sin\omega T_{L,W}}{\omega T_{L,W}}\exp(-i\omega T_{L,W}),\\ s_{L,W}(t)&=[H(t)-H(t-2T_{L,W})]/2T_{L,W}\end{aligned}\right\} \qquad (7)$$

It is clear from eqs. (5) and (7) that each of the deconvolved functions, $\Delta\dot{u}(t)$, $s_L(t)$, and $s_W(t)$ is a rectangular pulse with the width of τ, $2T_L$ and $2T_W$ respectively. $s(t)$ is a convolved pulse of $s_L(t)$ and $s_W(t)$, having a form of trapezoid specified at the time interval $0\leq t\leq 2(T_L+T_W)$ (HIRASAWA and STAUDER, 1965). $u_r^0(t)$ is a convolution of $\Delta\dot{u}(t)$ with $s(t)$, so that this has such a form as schematically shown in the lower part of Fig. 2.

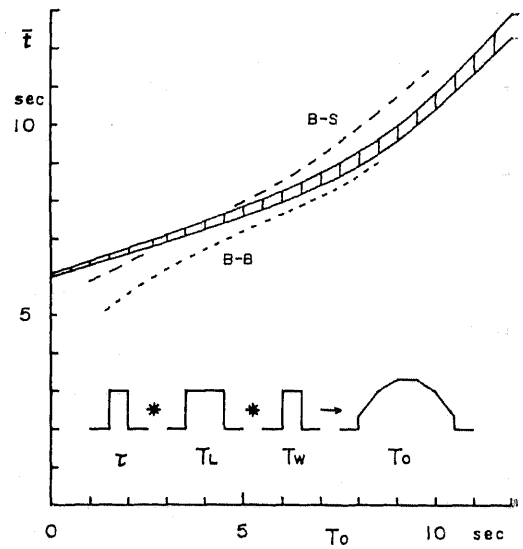

Fig. 2. Relation between first half-periods and the source process times.

The width of the base of the pulse, hereafter termed as the source process time T_0, is specified by,

$$T_0=\tau+2(T_L+T_W)=2\frac{d\tilde{\varphi}}{d\omega} \qquad (8)$$

As a next step, we shall determine T_0 in the time domain from observed records. In the lower half of Figs. 1(a) and 1(b), the times $\tilde{t}$ of the first half-cycle of P waves, which have been read directly on the vertical component seismograms at each station, are plotted by solid circles. We notice that there are parallel alignments between $\tilde{t}$ and $d\tilde{\varphi}/d\omega$, and hence this shows that $\tilde{t}$ can be used as a measure of T_0. It is now necessary to find a relationship between $\tilde{t}$ and T_0. The procedure emloyed here is similar to that used by BOLLINGER (1968, 1970). An empirical relation is established here on a number of hypothetical seismograms, which have been constructed by the convolution of $u_r^0(t)$ for variously assumed values of T_0 with the impulse response $h(t)$ of the earth-instrument system. Since the form of $u_r^0(t)$ is not uniquely specified only by the total time of T_0 but depends also on the partition of the time to τ, $2T_L$ and $2T_W$, so that computations have been made for various combinations of the

three parameters within their probable ranges. Fig. 2 shows an example of the relation for station HKC ($\Delta \simeq 40°$, $\Phi = 314°$ in earthquake No. 15), with a standard single-layered crust, an average attenuation of $T/\bar{Q}=1.5$ and with instrumental constants in the conventional system. The hatched part indicates a possible range of $\tilde{t}$ for an input of T_0. Although this kind of relation has to be derived for each station, the above example may be applied, as a first approximation, to most of the stations, to recover T_0 from $\tilde{t}$ since differences in crustal structures and attenuations do not yield significant discrepancies in the waveform. Two broken lines B-B and B-S show the relations derived by BOLLINGER (1970) for an incident box-car pulse and half-cosine pulse respectively. However, his relations, do not include the effects of attenuations and of the partition of the total time duration, and are

Table 2. Source process times and direction cosines

Station	α_1	α_2	α_3	To	Station	α_1	α_2	α_3	To
No. 15					No. 12				
2 COL	−0.290	−0.905	0.171	4.3	1 CMC	−0.810	−0.194	0.549	4.2
3 CMC	−0.270	−0.920	0.146	7.6	2 GSC	−0.854	−0.278	0.433	2·1
4 COR	−0.370	−0.909	0.049	6.5	3 TUC	−0.850	−0.356	0.380	2.5
5 BKS	−0.392	−0.907	−0.014	6.7	4 AFI	−0.952	−0.264	−0.155	4.2
6 KIP	−0.563	−0.818	0.016	3.6	5 WEL	−0.113	−0.972	0.199	0.
7 AFI	−0.630	−0.737	−0.372	4.6	6 SBA	−0.244	−0.857	0.448	0.
8 RIV	−0.113	−0.735	−0.766	5.4	8 MUN	−0.070	−0.483	0.871	0.8
9 MAN	0.345	−0.789	0.413	4.6	9 RAB	−0.355	0.179	0.917	1.8
10 BAG	0.323	−0.793	0.421	4.6	10 PMG	−0.197	0.044	0.979	7.7
11 HKC	0.286	−0.822	0.390	0.	12 BAG	−0.424	−0.085	0.900	3.1
12 NDI	0.235	−0.928	0.171	3.1	13 NHA	−0.383	−0.174	0.905	0.
13 LAH	0.213	−0.934	0.170	1.5	14 CHG	−0.434	−0.223	0.870	2.1
14 QUE	0.201	−0.947	0.382	2.0	15 HOW	−0.459	−0.263	0.846	1.5
15 NHA	0.413	−0.836	0.266	2.3	16 SHL	−0.477	−0.246	0.841	4.0
16 MUN	0.398	−0.823	−0.492	0.	20 ADE	0.048	−0.553	0.830	2.1
17 SEO	0.019	−0.810	0.471	4.8	21 ALQ	−0.846	−0.355	0.390	2.4
No. 6					No. 23				
1 HNR	−0.897	−0.385	0.231	4.0	1 RAB	−0.114	−0.797	0.487	2.0
2 RAB	−0.874	−0.370	0.325	1.4	2 PMG	−0.366	−0.722	0.393	0.2
3 PMG	−0.898	−0.259	0.361	1.4	3 BAG	−0.145	−0.567	0.685	1.8
4 CTA	−0.888	−0.089	0.448	1.4	4 HKC	−0.147	−0.519	0.715	3.8
5 MAN	−0.776	−0.396	0.502	1.4	5 NHA	−0.244	−0.507	0.666	2.6
6 SEO	−0.681	−0.544	0.508	2.2	6 SHL	−0.192	−0.406	0.750	2.2
7 BAG	−0.765	−0.422	0.498	1.9	7 HOW	−0.219	−0.388	0.742	2.5
8 ANP	−0.740	−0.459	0.506	2.7	8 KOD	−0.200	−0.452	0.723	2.8
9 HKC	−0.788	−0.407	0.474	1.5	9 LEM	−0.432	−0.443	0.561	0.7
10 KIP	−0.296	−0.875	0.418	0.6	10 MUN	−0.640	−0.270	0.429	1.1
11 COR	−0.302	−0.760	0.603	0.8	11 ADE	−0.754	−0.141	0.318	0.2
12 DUG	−0.267	−0.744	0.639	3.2	12 RIV	−0.823	−0.018	0.227	0.
13 GOL	−0.215	−0.721	0.685	3.6	13 SPA	−0.476	0.244	0.619	0.
14 LUB	−0.190	−0.708	0.706	3.4	14 SBA	−0.521	0.295	0.563	0.
15 ALQ	−0.224	−0.731	0.671	0.8	15 WEL	−0.559	0.517	0.413	2.7

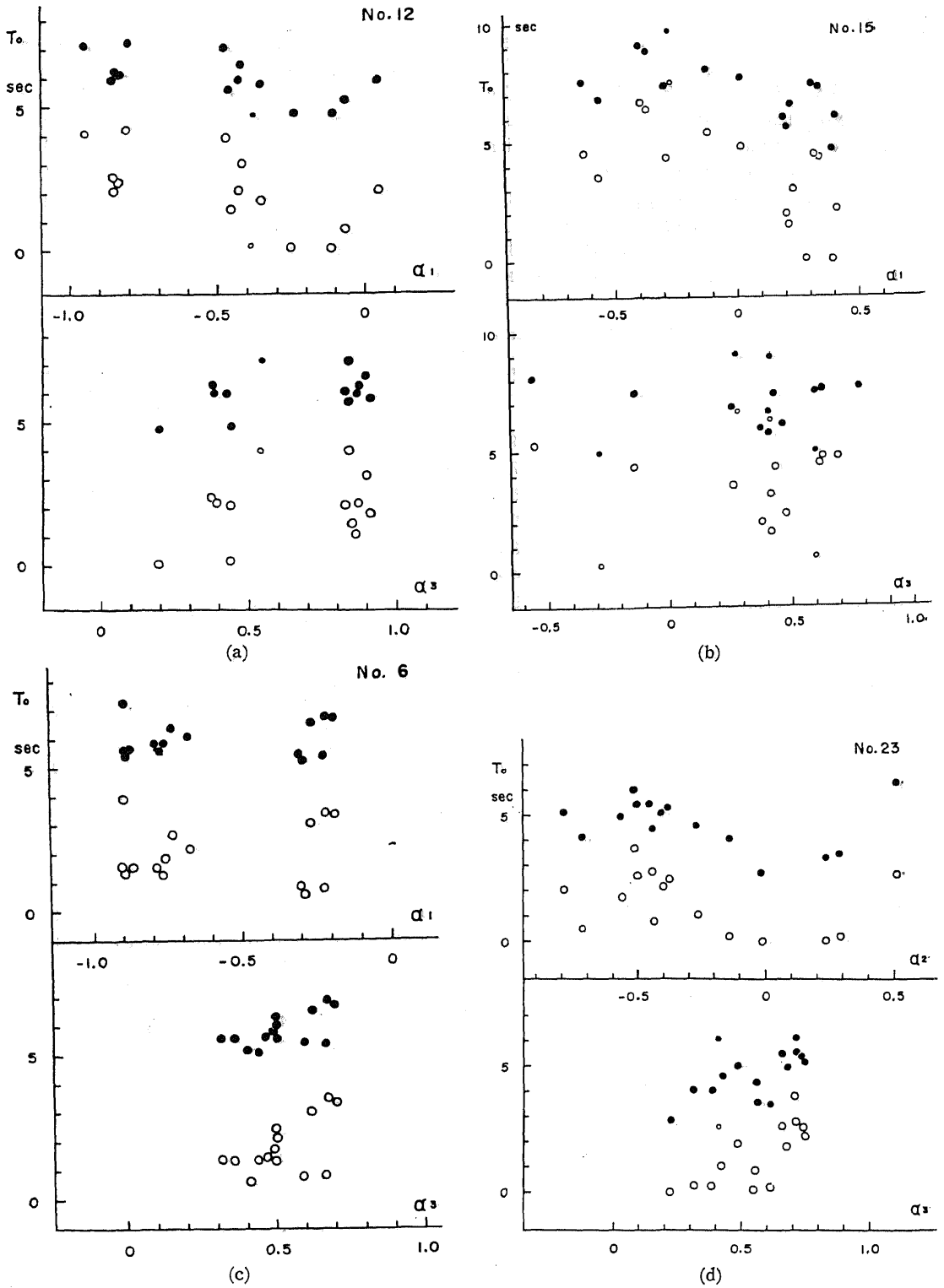

Fig. 3. Source process times plotted against the directions of one nodal plane and of the null vector. (a) No. 12 (b) No. 15 (c) No. 6 (d) No. 23

not used here.

The open circles plotted in the lower part of Figs. 1(a) and 1(b) are the source process times T_0 thus estimated from $\tilde{t}$ on the indivisual records. It can be seen that the plotted points show a good consistency with $2d\tilde{\varphi}/d\omega$ with less scattering. For this and the above stated reasons, we use the source process times obtained from this time domain analysis, rather than the group delay times from the frequency domain analysis to evaluate the source parameters.

§ 4. Estimation of Source Parameters

The source process times thus estimated at a number of stations for the four earthquakes are tabulated in Table 2, together with the direction cosines of the station azimuth with respect to the normals to two nodal planes and to the null vector respectively. The uncertainty of the process times due to measurement errors and to allowance in the relation between $\tilde{t}$ and T_0 is of the order of 0.5–1.0 sec. It is found that T_0 ranges from almost zero to about 4 sec and sometimes reaches 6 sec, although the average has been estimated as 2–3 sec (MIKUMO, 1969). Since differences in local crustal structures and in attenuations make only a difference of T_0 less than the above uncertainty, we take the interpretation that the rather large variations of T_0 result from azimuthally asymmetric source dimension and rupture propagation.

We shall now examine the possible azimuthal dependence of T_0. The dependence has been tested with respect to the three directions given in the above table, to determine which of the two nodal planes corresponds to the slip plane. It has been found for each of the four earthquakes, as shown in Figs. 3(a)~3(d), that there are some linear relations with considerable scatter between T_0 and either of the two directions (α_1 or α_2) to the nodal planes and also between T_0 and the direction (α_3) to the null vector. We conclude from the dependence that the nodal plane including the two relevant directions is the slip plane. The slip direction on this plane can be inferred from the radiation pattern of P wave first motions.

The next step is to evaluate four unknown source parameters L, W, τ and v. We also do not know the direction of rupture propagation at this stage. For this reason, we assume here that the rupture starts from a point and the front of it travels two-dimensionally at a constant velocity v as illustrated in Fig. 4(a). This assumption may be understood as bidirectional faulting (OTSUKA, 1964; HIRASAWA and STAUDER, 1965; FUKAO, private communication, 1970) in which the rupture propagates with different velocities along the longer and and shorter sides of the slip plane. In this case, eq. (8) may be rewritten in a more general form,

$$T_0=\tau+L_j\left|\frac{1}{v_j}-\frac{\alpha_j}{v_p}\right|+L_k\left|\frac{1}{v_k}-\frac{\alpha_k}{v_p}\right| \qquad (9)$$

where L_j and L_k are the linear source dimensions, and v_j and v_k are the apparent rupture velocities, as defined by $v_j=v/\sin\varphi$ and $v_k=v/\cos\varphi$, along the j- and k-directions, either of

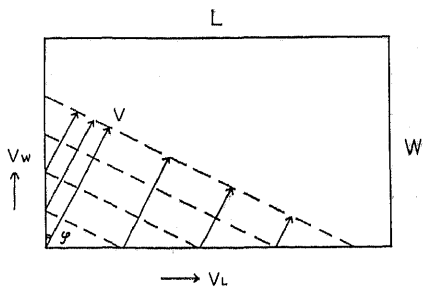

Fig. 4(a). Geometry for an assumed rupture process.

which corresponds to the slip direction and the other does to the orientation of the null vector. Eq. (9) indicates that there could be some different types of $T_0\sim\alpha_{j,k}$ diagram, as can be seen in Figs. 3(a)~3(d). 1) In case of $v_{j,k}<v_p$, the slope $\partial T_0/\partial\alpha_{j,k}$ should be negative if the rupture moves to the positive direction of the j- or k-axis, and positive for the rupture moving to the opposite direction. 2) In case of $v_{j,k}>v_p$; for stations with $\alpha_{j,k}<v_p/v_{j,k}<1$, the slope should be negative as in 1), but positive for stations with $v_p/v_{j,k}<\alpha_{j,k}<1$, being symmetric as to the axis of $\alpha_{j,k}=v_p/v_{j,k}$. The intercept time can take either positive or negative values.

Taking into account the above situations and re-arranging the sign of $\alpha_{j,k}$ for all stations, we determined three quantities L_j/v_p, L_k/v_p and $t_s=\tau\pm L_j/v_j\pm L_k/v_k$ by linear least squares for each earthquake. The computed results are:

	No. 6	No. 12	No. 15	No. 23
L_j/v_p	0.98±1.00	3.37±0.59	3.65±0.92	1.32±0.82
L_k/v_p	6.68±2.43	2.78±0.70	0.77±1.62	4.75±1.03
t_s	−2.28±1.84	−1.33±0.73	3.36±0.50	−1.81±0.92
δT_0	0.85	0.78	1.60	0.80

where the j- and k-axes were taken as the slip direction and the null vector respectively, and δT_0 shows the standard deviation of T_0.

From the above, the source dimensions L_j and L_k can be estimated with rather large uncertainty by assigning an appropriate value to the compressional velocity around the source region. The estimated length L (the longer one of the two length L_j and L_k) of the slip plane ranges from 25 to 42 km, while its width W (the shorter one of L_j and L_k) is about 6 to 20 km, being the order of 1/2~1/4 of the length, except for earthquake No. 12. The results show that the slip plane has a longer dimension in the slip direction for earthquake No. 15, but it does in the direction of the null vector for earthquakes Nos. 6 and 23. In the case of earthquake No. 12, the dimension has a comparable order in the two directions.

Once the dimensions were determined, the amount of dislocation D can also be estimated from the seismic moment or DLW, which has been determined in the previous paper (1969; See also Corrections, 1970) from comparison between the double amplitudes of the recorded and synthesized P waves. The estimated amount is 70~100 cm for three earthquakes and reaches 140 cm for earthquake No. 15.

On the other hand, we cannot uniquely determine τ and v by the least squares. It is possible, however, to estimate the probable ranges of the two parameters from t_s. Here we suppose two extreme cases: in case (A), the rupture is propagated along the longer direction L of the slip plane ($\varphi=\pi/2$, $v_W=\infty$); in case (B) the rupture is assumed to move along the shorter direction W ($\varphi=0$, $v_L=\infty$). Fig. 4(b) shows the relation between τ and $v_{L,W}$ in the two cases for the four earthquakes respectively, where two curves from one earthquake give the upper and lower bounds

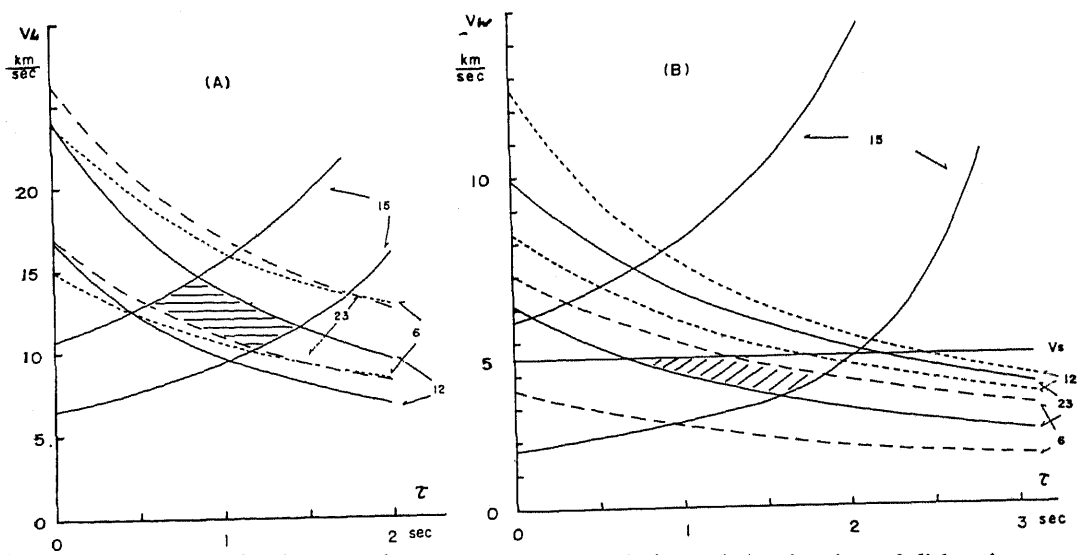

Fig. 4(b). Relation between the apparent rupture velocity and the rise time of dislocation.

that come from probable errors in the adopted dimension. If all the four earthquakes occur through the dynamical process with similar time constants and rupture velocities, τ and $v_{L,W}$ would fall in the hatched region bounded by the above curves. Case (A) indicates a region of $0.7<\tau<1.4$ sec and $10<v_L<14$ km/sec. Case (B) shows rather wide range. If we take the lowest value of τ as estimated in Case (A), a region of $0.7<\tau<1.8$ sec and $3.3<v_W<5.5$ km/sec sec will be bounded, except for earthquake No. 12. The lowest bound of the relation for the last earthquake does not go through the hatched region, but v_W would take similar values if τ exceeds 1.7 sec. Using these estimates for the two cases, we have $3.2<v<5.1$ and $13°<\varphi<29°$ from the relations $1/v^2=1/{v_L}^2+1/{v_W}^2$ and $\tan\varphi=v_W/v_L$, where φ is measured from the shorter side of the slip plane. If we further impose a limitation that the rupture velocity cannot exceed the shear wave velocity (MANSINHA, 1964), their possible values are $3.2<v<v_s\approx4.5$ km/sec and $13°<\varphi<24°$ respectively.

The stress drop during these earthquakes has also been estimated by using the obtained source parameters. For a dip-slip displacement along an infinitely long fault, $\Delta\sigma=(16/3\pi)\mu\bar{D}/W$ (AKI, 1966), while for an infinitely long vertical fault with strike-slip displacement, $\Delta\sigma=(2/\pi)\mu\bar{D}/W$ (KNOPOFF, 1958), where $\bar{D}$ as defined by $\bar{D}=(\pi/4)D_m$ is the average displacement over the entire fault surface. Earthquake No. 15 would correspond to the former case, and the latter may be applied to earthquakes Nos. 6, 12 and 23. The above equations assume, however, an infinitely long fault. It may be more appropriate to consider a circular crack with a finite radius a. For this type of dislocation, $\Delta\sigma=(7\pi/16)\mu\bar{D}/a$ (ESHELBY,

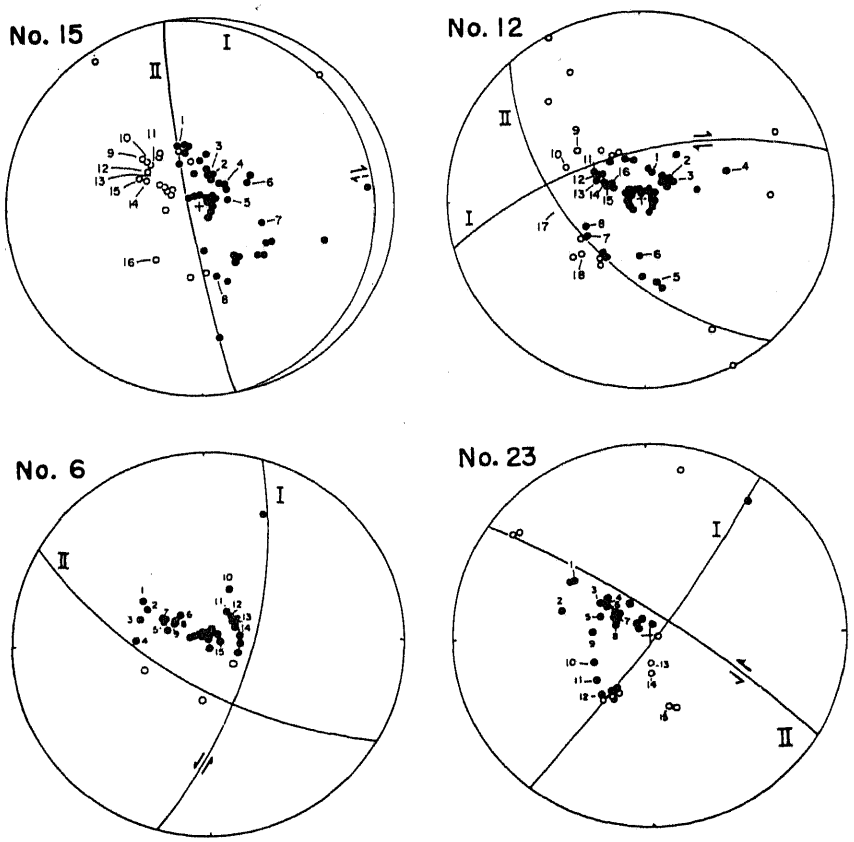

Fig. 5. Fault-plane solutions.

Table 3. Estimated source parameters.

	No. 15	No. 12	No. 6	No. 23
Slip plane	I	I	I	II
Fault length L (km)	(1) 29–37	(1) 25–32	(3) 34–42	(3) 27–37
Fault width W (km)	(3) 6–12	(3) 14–20	(1) 13–16	(2) 11–14
Moment M_0 (dyne·cm)	1.8×10^{26}	3.0×10^{26}	1.9×10^{26}	1.6×10^{26}
Dislocation D (cm)	(1) 110–140	(1) 75–100	(1) 80–100	(2) 55–75
Stress drop $\Delta\sigma$ (bar)	85–172	51–91	53–82	44–78
Rise time τ (sec)	0.7–1.4	same as in No. 15		
Rupture velocity v (km/sec)	3.2–4.5			

1957; KEYLIS-BOROK, 1959). The stress drop based on the last assumption (a was taken here as $a=\sqrt{A/\pi}$) are included in Table 3. The stress drop during earthquake No. 15 might reach 170 bar, while the other three earthquakes show similar values.

All the estimated source parameters of the four earthquakes are given in Table 3. The uncertainties in L and W have been reduced on the condition that τ and v take similar values for the four shocks. Fig. 5 illustrates their fault-plane solutions projected onto the lower hemisphere of the Wulff net, in which the slip direction is indicated by arrows.

§ 5. Comparison between Observed and Synthesized Seismograms of *P* and *S* Waves

In the previous study, the synthesized seismograms of P waves have been compared with the vertical component records at 15 stations in each of the four earthquakes analyzed here. There remains, however, an important problem whether observed S waveforms including the absolute amplitudes could also be explained by the dislocation sources derived from P waves. It has long been recognized from observations that predominant periods of S waves are usually longer than those of P waves, but it does not always appear from theoretical work (HASKELL, 1964; HIRASAWA and STAUDER, 1965) that moving dislocation models could fully account for the observational results. In this section, theoretical seismograms of S waves, as well as of P waves, are synthesized on the basis of the source parameters estimated in the preceding section, taking into account the effects of attenuation, and compared with their recorded waveforms on the three components.

The general solutions for the displacement of P and S waves from moving dislocation sources have been given by MARUYAMA (1963), HASKELL (1964), and BURRIDGE and KNOPOFF (1964), and treated in detail for the far field solutions by HIRASAWA and STAUDER (1965) and SAVAGE (1965). It is more convenient for practical purposes here to write the solutions referring to the geographical coordinate at the source. The m-component of the displacement of P and S waves in an infinite homogeneous medium may be written as, from their solutions,

$$\left.\begin{aligned} u_m &= u_m{}^p + u_m{}^s \\ u_m{}^p &= (2r_1r_2r_m/r^3)\cdot(v_s/v_p)^2\cdot u_0{}^p(t)/4\pi v_p r \\ u_m{}^s &= (\delta_{m2}r_1/r+\delta_{m1}r_2/r-2r_1r_2r_m/r^3)\cdot u_0{}^s(t)/4\pi v_s r \end{aligned}\right\} \quad (10)$$

where the suffixes p and s denotes the quantities for P and S waves. The 1- and 2-axes are taken to be perpendicular to the slip plane and parallel to the slip direction respectively. Using the notations in the previous study (MIKUMO, 1969),

$$\begin{aligned} u_0{}^{p,s}(t) &= \frac{DLW}{2\pi}\int_{-\infty}^{\infty}\dot{U}_D(\omega)\cdot S_D{}^{p,s}(\omega)\cdot e^{i\omega t}d\omega \\ &\equiv DLW\cdot I_{p,s} \end{aligned} \quad (11)$$

where

$$S_D(\omega)=S_1(\omega)\cdot S_2(\omega) \quad \text{and} \quad U_D(\omega)=\dot{U}(\omega)/D\,.$$

Here we introduce the geographical coordinate with the origin at the center of the source: $X=\sin\Theta\cdot\sin\Phi$, $Y=\sin\Theta\cdot\cos\Phi$, $Z=\cos\Theta$ (Θ and Φ are measured from the zenith and clockwise from the north). Let the displacement components, and the direction cosines of the 1-, 2-, and 3-axes, relative to the new coordinate be (u_X, u_Y, u_Z) and (l_m, m_m, n_m), respectively. Then we have

$$\left.\begin{aligned} &u_X=\sum l_m u_m,\quad u_X=\sum m_m u_m,\quad u_Z=\sum n_m u_m \\ &r_m/r=l_m\sin\Theta\sin\Phi \\ &\qquad +m_m\sin\Theta\cos\Phi+n_m\cos\Theta \\ &\qquad\qquad (m=1,2,3) \end{aligned}\right\} \quad (12)$$

The displacements for the (r, Θ, Φ)-components, which corresponds to those of P, SV and SH waves, are

$$\left.\begin{aligned} u_r&=(u_X\sin\Phi+u_Y\cos\Phi)\sin\Theta+u_Z\cos\Theta \\ u_\Theta&=(u_X\sin\Phi+u_Y\cos\Phi)\cos\Theta-u_Z\sin\Theta \\ u_\Phi&=u_X\cos\Phi-u_Y\sin\Phi \end{aligned}\right\} \quad (13)$$

where these components are taken positive in the directions away from the origin, away downwards for $\Theta<\pi/2$, and clockwise, respectively. Putting eqs. (10) and (12) into (13), we obtain,

$$\left.\begin{aligned} u_r&=c_p M_0 I_p/4\pi\rho v_p{}^3 r \\ u_\Theta&=c_{SV} M_0 I_S/4\pi\rho v_S{}^3 r \\ u_\Phi&=c_{SH} M_0 I_S/4\pi\rho v_S{}^3 r \end{aligned}\right\} \quad (14)$$

where

$$\left.\begin{aligned} &c_p=2\alpha_1\alpha_2,\quad c_{SV}=\alpha_1\beta_2+\alpha_2\beta_1,\quad c_{SH}=\alpha_1\gamma_2+\alpha_2\gamma_1 \\ &\alpha_m=l_m\sin\Theta\sin\Phi+m_m\sin\Theta\cos\Phi+n_m\cos\Theta \\ &\beta_m=l_m\cos\Theta\sin\Phi+m_m\cos\Theta\cos\Phi-n_m\sin\Theta \\ &\gamma_m=l_m\cos\Phi-m_m\sin\Phi \end{aligned}\right\} \quad (15)$$

c_p, c_{SV}, and c_{SH} are the constants specified by the source mechanism and the location of the relevant station, and equal to those in the case of double-couple point source (MIKUMO, 1962). M_0 is the seismic source moment defined as $M_0=\mu DLW$.

The amplitude distribution of P, SV and SH waves can be evaluated from eqs. (14) and (15), since the orientation of two nodal planes have been determined from the first motion pattern of P waves. Figs. 6(a) and 6(b) shows the distribution of first motion sings of c_p, c_{SV} and c_{SH} for the three kinds of body waves, together with their nodal curves, in two earthquakes Nos. 12 and 15, according to the

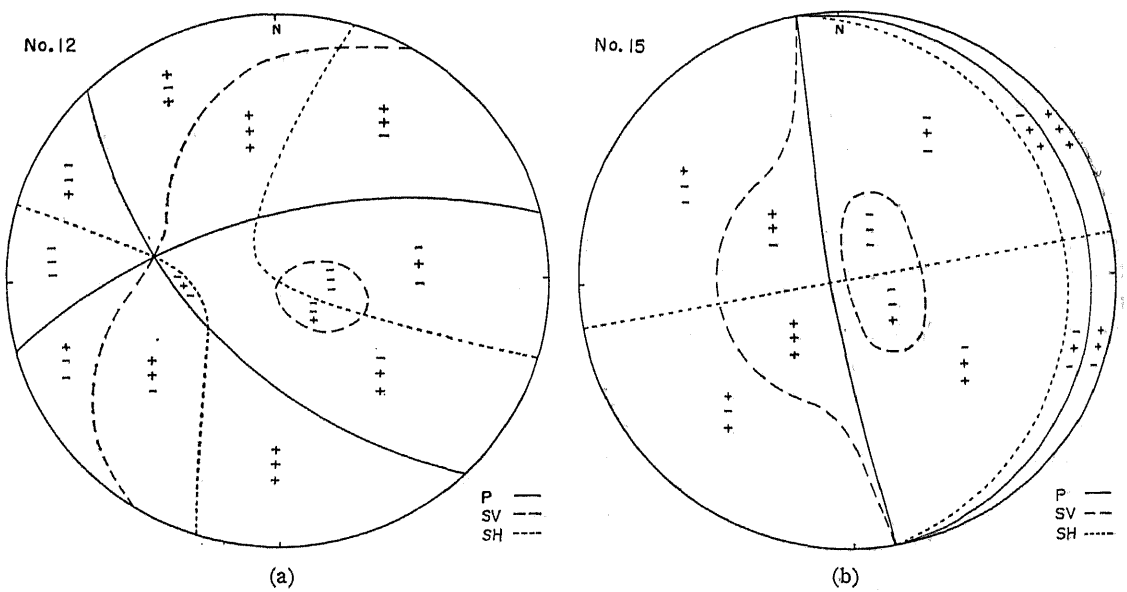

Fig, 6. Nodal curves of P, SV and SH waves.
(a) No. 12 (b) No. 15

method of KEYLIS-BOROK (1957). *SV* waves emitted downward from the source changes the sign during propagation to the station. This effect is included in the above figures. The above figures will be useful for the synthesis of the three components.

The body waves radiated from the source are suffered from the effects of propagation through the mantle and crust and of the seismograph. The waveforms that would be recorded on seismograms at the earth's surface should be derived from the superposition of normal modes in a gravitating spherical earth (for example, SATÔ *et al.*, 1967; USAMI *et al.*, 1968). It has been shown (SATO, 1969), however, that for direct body waves with periods probably up to about 40 sec, the divergence effect for a limited but rather wide range of epicentral distances may be approximated with errors less than 5% by the geometrical spreading expected from the ray theory. For this reason, the waveforms may be expressed, to a good approximation, by (MIKUMO, 1969)

$$f_{P,SV,SH}(t)=\int_0^\infty u_{r,\theta,\phi}(\tau)\cdot r\cdot h_{p,s}(t-\tau)d\tau$$
$$=\int_{-\infty}^{\infty} U_{r,\theta,\phi}(\omega)\cdot H_{p,s}(\omega)e^{i\omega t}d\omega \qquad (16)$$

where

$$h_{p,s}(t)=\frac{1}{2\pi}\int_{-\infty}^{\infty} H_{p,s}(\omega)e^{i\omega t}d\omega$$

and

$$H_{p,s}(\omega)=P_{p,s}(\omega)\cdot C_{p,s}(\omega)\cdot I(\omega)$$

$P(\omega)$, $C(\omega)$, $I(\omega)$ and $H(\omega)$ are the mantle transfer function, crustal response, instrumental response and the total system response, respectively. $P(\omega)$ for direct S waves has been computed here by the product of geometrical spreading and attenuation from the Jeffreys-Bullen velocity profile and probable dissipative models, as in the case of direct P waves. For attenuation effect, we refer mainly to a Q model (Model 11) of MIKUMO and KURITA (1968) by reducing the Q values by a constant rate of 4/9 at all depths according to a relation $Q_\alpha/Q_\beta=9/4$ suggested by ANDERSON *et al.* (1965), and also to their MM8-Q_β model for the sake of comparison. $C(\omega)$ has also been computed for the vertical and horizontal components of P and SV waves and for SH waves by the matrix method (HASKELL, 1960, 1962), for the layered structure appropriate to each station and for the pertinent incident angle. When the structure is not known, the unilayered model of HASKELL has been applied to the stations.

Now we have the synthesized seismograms of the vertical and horizontal components of P and SV waves $f_{Pu}(t)$, $f_{Pw}(t)$, $f_{SVu}(t)$ and $f_{SVw}(t)$, and of SH waves, $f_{SH}(t)$, through eq. (16). Fig. 7 shows the observed (full line) and synthesized (broken line) waveforms on the vertical component seismograms for five

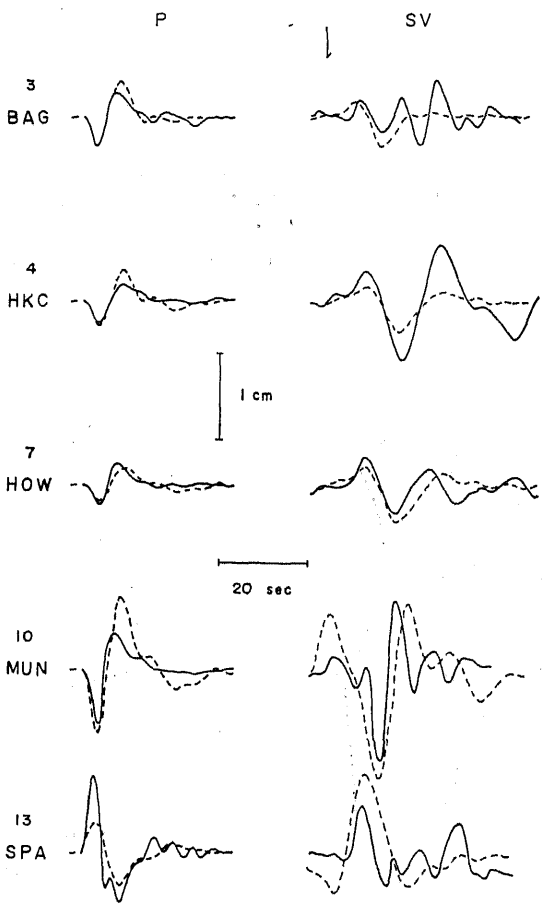

Fig. 7. Observed and synthesized seismograms of earthquake No. 23. (vertical component of P and SV waves)

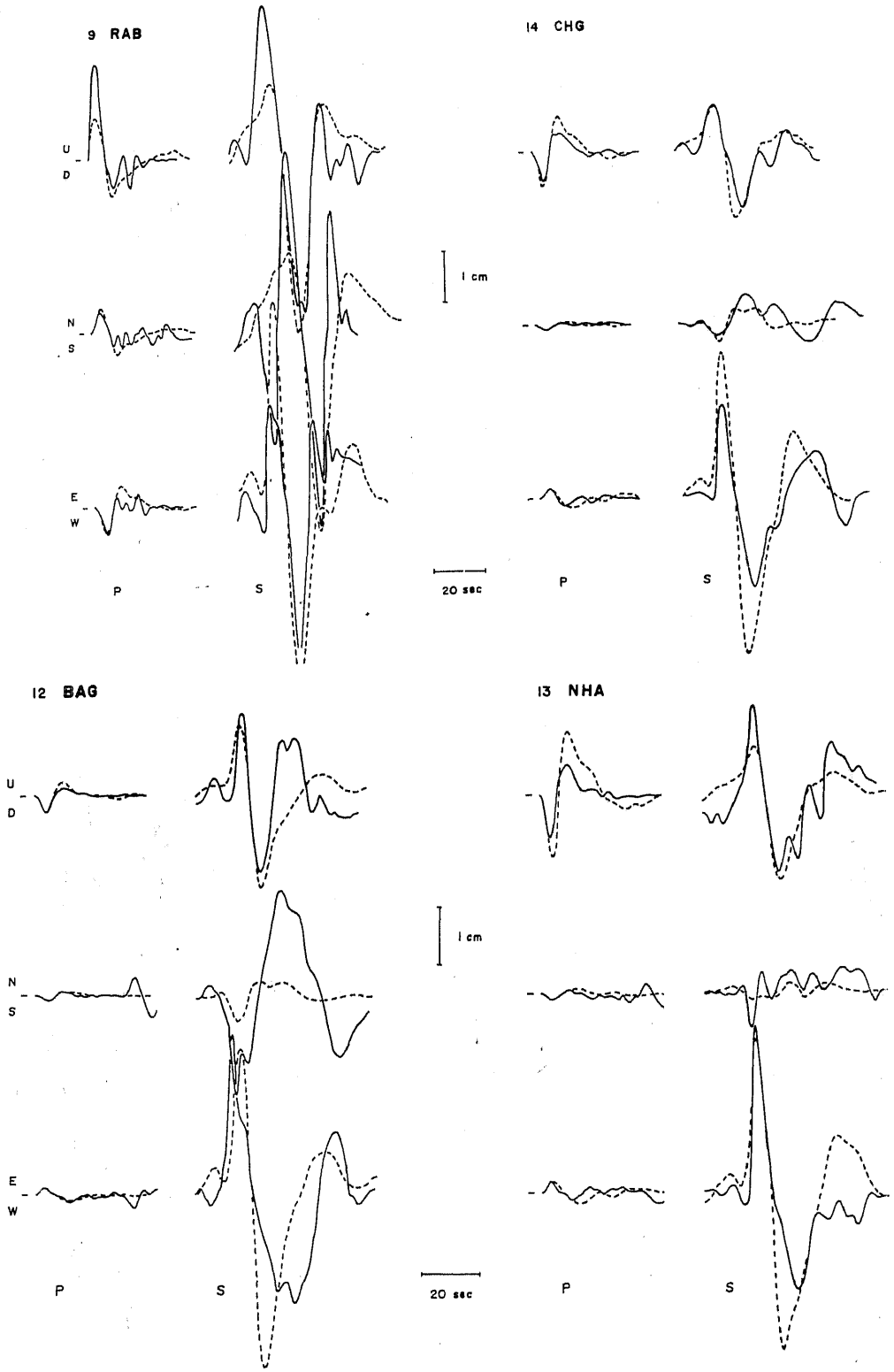

Fig. 8(a)

Fig. 8. Observed and synthesized seismograms (three components of P and S waves). (a) earthquake No. 12.

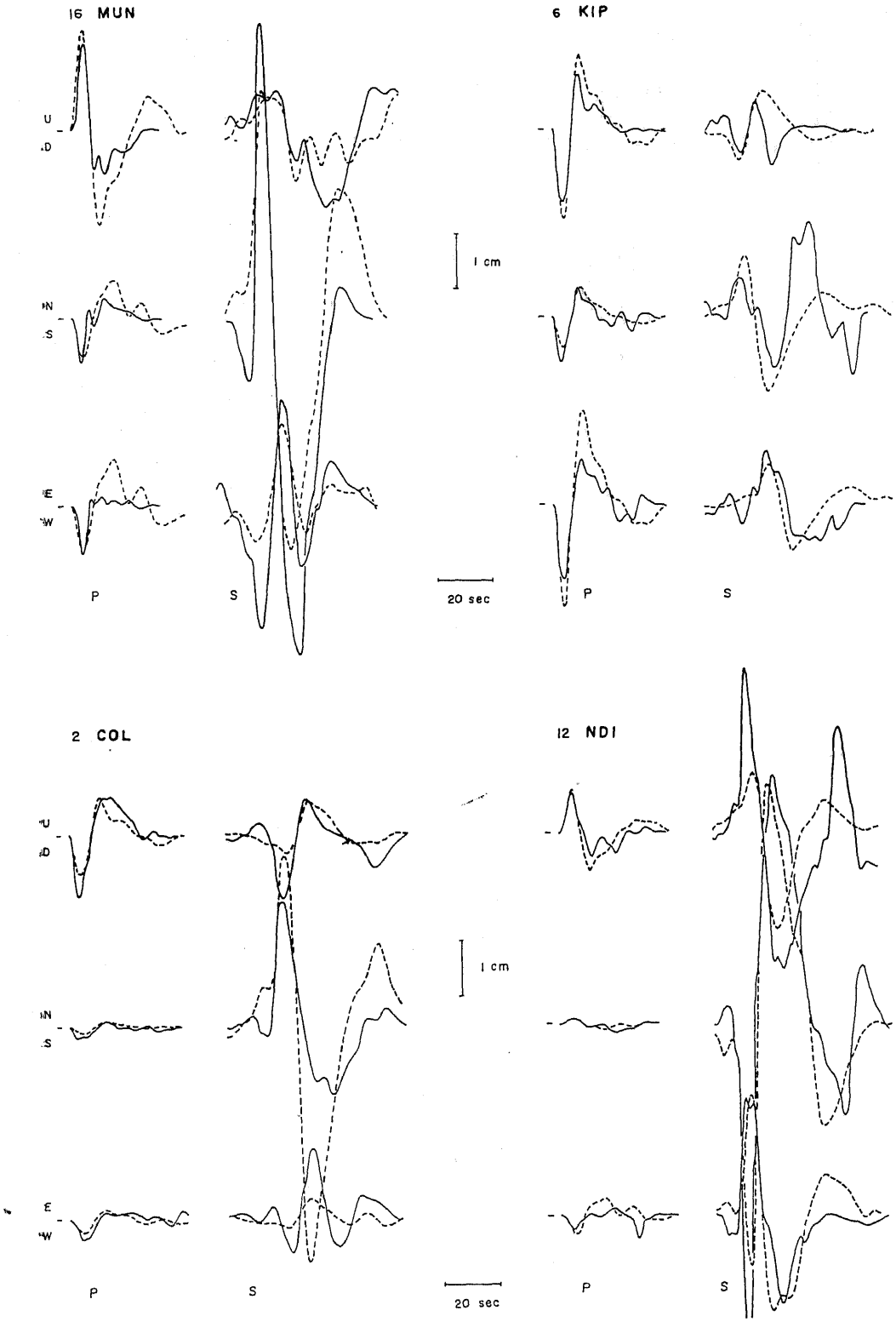

(b)

Fig. 8. Observed and synthesized seismograms (three components of P and S waves) (b) earthquake No. 15.

selected stations in earthquake No. 23. It appears that general features of the waveforms are in good agreement between the two kinds of seismograms. The S waves recorded at MUN and SPA show rather shorter periods than those predicted. If the short-period oscillations are removed by a proper filtering, the agreement would be much improved.

It is more appropriate to make such a comparison on the three component seismograms, since a different kind of information is involved in the horizontal records, particularly of S waves. It is, however, usually difficult to see well-isolated direct S waves on all of the three components at many stations. This is because they are often contaminated by preceding motion of P wave group and later phases such as sS and ScS over a wide range of epicentral distances, and partly because SV waves are sometimes distorted by the crust due to large incident angles. For this reason, the comparison can be made only for a limited number of stations, whereas FUKAO (1970) estimated the fault parameters directly from S waveforms at many stations.

Two horizontal components $f_N(t)$ and $f_E(t)$ on the synthesized seismograms are derived by the rotation of axis,

$$\left.\begin{aligned} f_N(t)&=f_{Pu}(t)\cos\varphi \\ f_E(t)&=f_{Pu}(t)\sin\varphi \quad \text{for } P \text{ waves} \end{aligned}\right\} \text{and} \left.\begin{aligned} f_N(t)&=f_{SVu}(t)\cos\varphi+f_{SH}(t)\sin\varphi \\ f_E(t)&=f_{SVu}(t)\sin\varphi-f_{SH}(t)\cos\varphi \\ &\qquad \text{for } S \text{ waves} \end{aligned}\right\} \quad (17)$$

respectively, where φ is the back azimuth measured from station to epicenter. Figs. 8(a) and 8(b) depict the recorded (full line) and synthesized broken line three component seismograms of both P and S waves at four stations for earthquakes Nos. 12 and 15. All the seismograms have been normalized to a seismograph magnification of 1,500.

It may be seen that there is general agreement between the observations and theoretical predictions for most of the P and S waveforms. An introduction of MM8-Q_β model instead of the Q_β model assumed here did not make much difference in the S wave amplitudes. It was also found that an arbitrary assumption of $Q_\alpha=Q_\beta$ makes the theoretical S-wave amplitude significantly larger than the recorded amplitudes. An appreciable discrepancy lies, however, in the NS-component of S waves at BAG in earthquake No. 12 and at COL in earthquake No. 15. It is likely that the discrepancy comes from the wave incidence deviating from the great circle path. There is also a possibility that different attenuations for SV and SH waves could reconcile the discrepancy. However, most acceptable explanations would be that the S-wave amplitudes at the two stations are sensitive to the accuracy of the fault plane solutions, since the stations are located near the nodal plane of SV waves (Compare Fig. 5 with Figs. 6(a) and 6(b)). Although there are also some differences in the amplitudes for specific peaks or troughs, it may be said that the recorded and synthesized waveforms of P and S waves, including their amplitudes, are in good agreement. Also, the predominant periods of the synthesized S waves are apparently longer than those of P waves, and generally agree with the observed periods. This may be accounted for mainly by higher attenuations in the mantle and partly by longer source process times due to combined effects of the fault length and width.

It may be concluded from the above comparison that the observed S waveforms including the absolute amplitudes give support to the dislocation sources inferred from P waves.

§ 6. Discussion

In this paper, we have estimated various source parameters for shear dislocation models. There are alternative hypotheses for deep-focus earthquakes, such as volume changes due to phase transitions (BENIOFF, 1963; DENNIS and WALKER, 1965; RANDALL, 1966; EVISON, 1967) and tensile fracture (or extentional dislocation) models (SAVAGE, 1965;

BURRIDGE, 1968). It appears, however, that azimuthal dependence of the source process times as well as the radiation patterns of the double-couple type, which were found here, favor the shear dislocation models for the four earthquakes analyzed. This does not necessarily mean that the source process of all deep earthquakes can be related to shear dislocations. More deep earthquakes in different regions need be analyzed to test the validity of this model.

We have so far assumed bidirectional type of faulting rather than pure unilateral and bilateral, since it may be more realistic to consider that faulting would initiate near the center of the stressed region (SAVAGE, 1966) and proceed rapidly on the fault surface along and across the slip directions, in view of a number of evidence that aftershocks of large shallow earthquakes occur frequently in an area with the main shock at the edge.

If we suppose that unilateral faulting propagates along the longer axis of the slip plane (Case (A)), it would follow that the rupture velocity takes unusually high values. FUKAO (1970) also obtained an extremely high rupture velocity for a deep-focus earthquake of Banda Sea from the analysis of S waveforms. In these cases, we would have to take the following interpretations. One would be simultaneous faulting; the source process will be such that body waves are radiated almost simultaneously over the entire fault surface within the rise time of dislocation (FUKAO, 1970). The source process time in this case is interpreted as the time difference between the arrival time of body waves from the nearest point on the fault surface at the initiation of the rupture process and that from the farthest point at the termination (FUKAO, 1970). Another interpretation would be supersonic dislocations, in which the rupture velocity exceeds elastic wave velocities. The possibility has been suggested by ESHELBY (1956) for a part of screw dislocation on a slip plane in crystals, and by WEERTMAN (1969) for slippage for earthquake faults. WEERTMAN (1969) has proved that both screw dislocations and edge dislocations over an infinite distance could move at a uniform supersonic velocity on a slip or fault plane, if the frictional stress decreases with increasing displacement velocity across the slip plane.

If we assume bilateral faulting, the total process time is the superposition of the width of two pulses from two unilateral faulting in opposite directions. Since a predominant portion with large amplitude usually lies in the first-arrived pulse, the synthesized waveform is between those from the two unilateral faulting (MIKUMO, 1969). It would be difficult, therefore, to discriminate bilateral faulting from unilateral one on the azimuthal dependence of the source process times.

The concept of bidirectional faulting has been introduced by FUKAO (private communication, 1970) in the time domain analysis of a multiple deep-focus shock in South America. It has been demonstrated that this type of faulting could account for our results, particularly for the rupture velocity. It appears that the rupture has propagated at velocities between 3.2 and a shear velocity of 4.5 km/sec in the present case, as has been suggested by a theoretical work (MANSINHA, 1964) and from a number of observations. The propagating direction makes a small angle to the shorter axis of the fault plane. If these interpretations are correct, earthquakes Nos. 6 and 23 with predominant strike slip component would be approximated by edge dislocations, while earthquake No. 12 having strike-slip with a fraction of dip-slip component, and earthquake No. 15 characterized by thrust faulting could be associated with screw dislocations.

We shall next estimate the effective stress at the initial state to produce slip dislocations from the results in the preceding sections. OROWAN (1960) has stated that during the fault rupture a frictional stress σ_f acts to resist the fault slippage, and the initial shear stress σ_a decreases to σ_f when the slippage will cease. Since, in this case, an amount of the energy $\sigma_f DA$ will be lost as frictional heating, while an energy $\frac{1}{2}(\sigma_a - \sigma_f)DA$ will go into the generation of seismic

waves, the stress deduced from seismic waves is the average effective stress $\sigma_a - \sigma_f$ (BRUNE, 1970). Although it is difficult to determine the stresses σ_a and σ_f separately from seismic observations, the effective stress may be inferred from the stress drop and the average acting stress. We have the following relation (AKI, 1966; BRUNE, 1968; WYSS and BRUNE, 1968) among the average acting stress $\bar{\sigma}$ (average of initial stress σ_1 and final stress σ_2), the seismic moment M_0, and the strain energy released E_0; $\bar{\sigma}=(\sigma_1+\sigma_2)/2=E_0/\bar{D}A=\mu E_0/M_0$, and $\eta\bar{\sigma}=\mu E_s/M_0$, where E_s and η are the seismic wave energy and efficiency respectively and $\eta\bar{\sigma}$ means a lower bound for the actual average stress. If we assume further that the total energy release is equal to the sum of the seismic and frictional energies, ie. $E_0=E_s+E_f$, it follows that $\bar{\sigma}=\eta\bar{\sigma}+\sigma_f$ (BRUNE *et al.*, 1969). The stress drop during the faulting process is $\Delta\sigma=\sigma_1-\sigma_2<\sigma_1$. Combing these relations, we have $\sigma_1-\sigma_f=\Delta\sigma/2+\eta\bar{\sigma}$ for the effective initial stress to produce shear dislocations.

The estimated stress drop at the time of the four intermediate earthquakes, as given in Table 3, seems slightly larger than that for shallow earthquakes with similar magnitudes (BRUNE and ALLEN, 1967; BRUNE, 1968), and considerably lower than that for deep-focus earthquakes (BERCKHEMER and JACOB, 1968; FUKAO, 1970), although their methods of estimates were different from ours. On the other hand, the apparent average stress $\eta\bar{\sigma}$ for the four shocks lies between 8 and 37 bars (MIKUMO, 1970). These values are of the same order with those for shallow and deep-focus earthquakes (WYSS and BRUNE, 1968; WYSS, 1970), while WYSS (1970) obtained 270 bars as the mean value for 10 intermediate earthquakes between 45 and 150 km in South America. He stated, however, that earthquakes at intermediate depths in the Tonga-Kermadec Trench are not characterized by such a high apparent average stress. From these evidence, it may be reasonable to consider that the effective initial shear stress at intermediate depths will be appreciably larger than those at the crust and the uppermost mantle. These high stresses may be due to high values of σ_1, or low values of σ_f, or both.

The high initial stress would be associated with high strength of material, although it does not appear to reach MCKENZIE's estimate of 2.5 kb for the stresses that could be accumulated in descending slabs of the lithosphere in deep seismic zones (MCKENZIE, 1969). The possible low frictional stress would occur in relation to the temperature-pressure relation. It is likely that increasing temperature at intermediate depths probably with the high stresses produce partial melting of material or a well-lubricated state on a slip plane (OROWAN; 1960: GRIGGS and BAKER, 1969), and hence this would decrease the dynamic frictional stress at the time of dislocations. The effective initial stress $\sigma_1-\sigma_f$ for the four earthquakes is estimated to be about 30~120 bars from the above derived relation.

It is to be noted that the above interpretations should be regarded as only tentative, and more deep and intermediate earthquakes need be analyzed.

Acknowledgments

I have benefited from stimulate discussions with Drs. Yoshio Fukao and Katsuyuki Abe of the Earthquake Research Institute, and Mr. Kazuo Oike at our Institute. I wish to thank Dr. Michio Otsuka of Kumamoto University for valuable suggestions at an early stage of this study. My thanks are also extended to Mrs. Ritsuko Koizumi for assistance in the present work. Computations were made on a FACOM 230-60 at the Data Processing Center, Kyoto University.

References

Aki, K., Generation and propagation of *G* wave from the Niigata earthquake of June 16, 1964, Part 2. Estimation of earthquake moment, released energy and stress-strain drop from the *G* wave spectrum, *Bull. Earthq. Res. Inst.*, **44**, 73-88, 1966.

Anderson, D. L., A. Ben-Menahem and C. B. Archambeau, Attenuation of seismic energy in the mantle, *J. Geophys. Res.*, **70**, 1441-1448, 1965.

Benioff, H., Source wave form of three earthquakes, *Bull. Seism. Soc. Amer.*, **53**, 893-904, 1963.

Berckhemer, H. and K. H. Jacob, Investigation of the dynamical process in earthquake foci by analyzing the pulse shape of body waves, *Proc. of the X Assembly of the ESC*, Sept., 1968, II, 253-352, 1970.

Bollinger, G. A., Determination of earthquake fault parameters from long-period *P* waves, *J. Geophys. Res.*, **73**, 785-807, 1968.

Bollinger, G. A., Fault length and fracture velocity for the Kyushu, Japan, earthquake of October 3, 1963, *J. Geophys. Res.*, **75**, 955-964, 1970.

Brune, J., Travel times, body waves and normal modes of the earth, *Bull. Seism. Soc. Amer.*, **54**, 2099-2127, 1964.

Brune, J., Seismic moment, seismicity, and rate of slip along major fault zones, *J. Geophys. Res.*, **73**, 777-784, 1968.

Brune, J., Tectonic stress and the spectra of seismic shear waves from earthquakes, *J. Geophys. Res.*, **75**, 4997-5009, 1970.

Brune, J. and C. R. Allen, A low stress-drop, low-magnitude earthquake with surface faulting: The Imperial, California, earthquake of March 4, 1966, *Bull. Seism. Soc. Amer.*, **57**, 501-514, 1967.

Brune, J. N., T. L. Henrey and R. F. Roy, Heat flow, stress and rate of slip along the San Andreas Fault, California, *J. Geophys. Res.*, **74**, 3821-3827, 1969.

Burridge, R. and L. Knopoff, Body force equivalents for seismic dislocations, *Bull. Seism. Soc. Amer.*, **54**, 1875-1888, 1964.

Burridge, R., Theoretical seismic sources and propagating brittle cracks, *J. Phys. Earth*, **16**, Special Issue, 83-92, 1968.

Dennis, J. G. and C. T. Walker, Earthquakes resulting from metastable phase transitions, *Tectonophysics*, **2**, 401-405, 1965.

Eshelby, J. D., Supersonic dislocations and dislocations in dipersive media, *Proc. Phys. Soc. London*, **B 69**, 1013-1019, 1956.

Eshelby, J. D., The determination of the elastic field of an ellipsoidal inclusion and related problems, *Proc. Roy Soc. London*, **A 241**, 376-396, 1957.

Evison, F. F., On the occurrence of volume change at the earthquake source, *Bull. Seism. Soc. Amer.*, **57**, 9-26, 1967.

Fukao, Y., Focal process of a deep focus earthquake as deduced from long-period *P* and *S* waves, *Bull. Earthq. Res. Inst.*, **48**, 707-727, 1970.

Griggs, D. T. and D. W. Baker, The origin of deep-focus earthquakes, in *Properties of Matter*, pp. 23-42, John Wiley & Sons, New York, 1969.

Haskell, N. A., Crustal reflection of plane SH waves, *J. Geophys. Res.*, **65**, 4147-4150, 1960.

Haskell, N. A., Crustal reflection of *P* and *SV* waves, *J. Geophys. Res.*, **67**, 4751-4767, 1962.

Haskell, N. A., Total energy and spectral density of elastic wave radiation from propagating fault, *Bull. Seism. Soc. Amer.*, **54**, 1811-1841, 1964.

Hirasawa, T. and W. Stauder, On the seismic body waves from a finite moving source, *Bull. Seism. Soc. Amer.*, **55**, 237-262, 1965.

Isacks, B, J. Oliver and L. R. Sykes, Seismology and the new global tectonics, *J. Geophys. Res.*, **73**, 5855-5899, 1968.

Keylis-Borok, V. I., The determination of earthquake mechanism, using both longitudinal and transverse waves, *Ann. Geofis.*, **10**, 105-128, 1957.

Keylis-Borok, V. I., On estimation of the displacement in an earthquake source and of source dimensions, *Ann. Geofis.*, **12**, 205-214, 1959.

Knopoff, L., Energy release in earthquakes, Geophys. J., **1**, 44-52, 1958.

Maruyama, T., On the force quivalents of dynamical elastic dislocations with reference to the earthquake mechanism, *Bull. Earthq. Res. Inst.*, **41**, 467-486, 1963.

Mansinha, L., The velocity of shear fracture, *Bull. Seism. Soc. Amer.*, **54**, 369-376, 1964.

McKenzie, D. P, Speculations on the consequences and causes of plate motions, *Geophys. J.*, **18**, 1-32, 1969.

Mikumo, T., Mechanism of local earthquakes in Kwanto region, Japan, derived from the amplitude relation of *P* and *S* waves, *Bull. Earthq. Res. Inst.*, **40**, 399-424, 1962.

Mikumo, T. and T. Kurita, *Q* distribution for long-period *P* waves in the mantle, *J. Phys. Earth*, **16**, 11-29, 1968.

Mikumo, T., Long-period *P* waveforms and the source mechanism of intermediate earthquakes, *J. Phys. Earth*, **17**, 169-192, 1969; Correction, *ibid.*, **18**, 313, 1970.

Orowan, E., Mechanism of seismic faulting in rock deformation, A Symposium, *Geol. Soc. Amer. Mem.*, **79**, 323-345, 1960.

Otsuka, M., Study on focal mechanism by the analysis of seismic waves of *S*-type, *Spec. Contr. Geophys. Inst., Kyoto Univ.*, **4**, 37-49, 1964.

Randall, M. J., Seismic radiation from a sudden phase transition, *J. Geophys. Res.*, **71**, 5297-5302, 1966.

Satô, Y., T. Usami and M. Landisman, Theoretical seismograms of spheroidal type on the surface of a gravitating elastic sphere, II. Case of Gutenberg-Bullen A′ earth model, *Bull. Earthq, Res. Inst.*, **45**, 601-624, 1967.

Sato, R., Amplitude of body waves in a heterogeneous sphere, comparison of wave theory and ray theory, *Geophys. J.*, **17**, 527-544, 1969.

Savage, J. C., The effect of rupture velocity upon seismic first motions, *Bull. Seism. Soc. Amer.*, **55**, 263-275, 1965.

Savage, J. C., Radiation from a realistic model of faulting, *Bull. Seism. Soc. Amer.*, **56**, 577-592, 1966.

Teng, T. L. and A. Ben-Menahem, Mechanism of deep earthquakes from spectrums of isolated body-wave signals, 1. Banda Sea earthquake of March 21, 1964, *J. Geophys. Res.*, **70**, 5157-5170, 1965.

Usami, T., Y. Satô and M. Landisman and T. Odaka, Theoretical seismograms of spheroidal type on the surface of a gravitating elastic sphere, III. Case of a homogeneous mantle with a liquid core, *Bull. Earthq. Res. Inst.*, **46**, 791-819, 1968.

Weertman, J., Dislocation motion on an interface with friction that is dependent on sliding velocity, *J. Geophys. Res.*, **74**, 6617-6622, 1969.

Wyss, M., and J. N. Brune, Seismic moment, stress, and source dimensions from earthquakes in the California-Nevada region, *J. Geophys, Res.*, **73**, 4681-4694, 1968.

Wyss, M., Stress estimates for South American shallow and deep earthquakes, *J. Geophys. Res.*, **75**, 1529-1544, 1970.

(Received September 29, 1970;
revised December 26, 1970)